Proc. Natl. Acad. Sci. USA
Vol. 93, pp. 1125–1129, February 1996
Biophysics

On the nucleation and growth of amyloid β-protein fibrils: Detection of nuclei and quantitation of rate constants

(Alzheimer disease/fibrillogenesis/light scattering)

ALEKSEY LOMAKIN[†‡§], DOO SOO CHUNG[†¶], GEORGE B. BENEDEK[†‖], DANIEL A. KIRSCHNER[‡,††,‡‡], AND DAVID B. TEPLOW[‡§‖]

[†]Department of Physics and Center for Materials Science and Engineering, Massachusetts Institute of Technology, Cambridge, MA 02139; [‡]Department of Neurology (Neuroscience), Harvard Medical School, Boston, MA 02115; [§]Biopolymer Laboratory, Brigham and Women's Hospital, Boston, MA 02115; and [††]Neurology Research, Children's Hospital, Boston, MA 02115

Contributed by George B. Benedek, October 23, 1995

ABSTRACT **We have studied the fibrillogenesis of synthetic amyloid β-protein-(1–40) fragment (Aβ) in 0.1 M HCl. At low pH, Aβ formed fibrils at a rate amenable to detailed monitoring by quasi-elastic light-scattering spectroscopy. Examination of the fibrils with circular dichroism spectroscopy and electron microscopy showed them to be highly similar to those found in amyloid plaques. We determined the hydrodynamic radii of Aβ aggregates during the entire process of fibril nucleation and growth. Above an Aβ concentration of ≈0.1 mM, the initial rate of elongation and the final size of fibrils were independent of Aβ concentration. Below an Aβ concentration of 0.1 mM, the initial elongation rate was proportional to the peptide concentration, and the resulting fibrils were significantly longer than those formed at higher concentration. We also found that the surfactant *n*-dodecylhexaoxyethylene glycol monoether ($C_{12}E_6$) slowed nucleation and elongation of fibrils in a concentration-dependent manner. Our observations are consistent with a model of Aβ fibrillogenesis that includes the following key steps: (*i*) peptide micelles form above a certain critical Aβ concentration, (*ii*) fibrils nucleate within these micelles or on heterogeneous nuclei (seeds), and (*iii*) fibrils grow by irreversible binding of monomers to fibril ends. Interpretation of our data enabled us to determine the sizes of fibril nuclei and Aβ micelles and the rates of fibril nucleation (from micelles) and fibril elongation. Our approach provides a powerful means for the quantitative assay of Aβ fibrillogenesis.**

Alzheimer disease is a progressive, neurodegenerative disorder characterized by amyloid deposition in senile plaques in the cerebral parenchyma and vasculature (1). These plaques are composed primarily of fibers of the amyloid β-protein fragment Aβ-(1–40) (Aβ) (1). Aβ is derived by proteolytic processing of the 110- to 130-kDa β-protein precursor (βPP) (2) within an acidic intracellular compartment such as the early endosome or distal Golgi complex (3, 4). Aβ is a normal constituent of human plasma and cerebrospinal fluid (5, 6) and, in culture, is secreted by a variety of cells, including primary neuronal and nonneuronal cells (7, 8). *In vivo*, senile plaques containing dense cores of fibrillar Aβ are intimately associated with areas of neuronal loss, dystrophic neurites, and gliosis (1). A number of studies have provided information on the structure of fibrils formed both *in vivo* and *in vitro* and on factors affecting fiber formation. Electron microscopy (EM) of amyloid plaques has revealed straight or slightly curved fibers 6–10 nm in diameter and of indeterminate length (9, 10). X-ray diffraction studies have demonstrated that these fibers have a cross-β-pleated-sheet structure (11). Synthetic Aβ peptides form fibers ultrastructurally indistinguishable from those isolated from the brain (12). Circular dichroism (CD) and Fourier-transform IR spectroscopic analyses of these synthetic fibers have confirmed their β-sheet secondary structures (13, 14). The ability of synthetic Aβ to form amyloid fibrils *in vitro* has been utilized to examine how a variety of parameters, including temperature, pH, solvent composition, peptide concentration, and peptide sequence influence the final fibril state (14–17). What is substantially less understood, however, is the kinetics of Aβ fibril growth.

Quantitative kinetic studies of Aβ fibrillogenesis have been complicated by the fact that fibril formation typically occurs very rapidly and is sensitive to variations in the method of preparation of the initial Aβ stock solutions (18–20). Although recent work has demonstrated that exogenous proteins and chemicals can affect Aβ fibrillogenesis *in vitro*, the nature of these effects is not entirely clear. For example, apolipoprotein E4 and α_1-antichymotrypsin both have alternately been reported to "promote" (21, 22) and to "inhibit" or destabilize (23–25) amyloid fibril formation.

Fibrillization of many proteins [for example, of actin (26–28)], is controlled by two kinetic parameters: the nucleation rate and the growth rate. Consequently, simple terms such as "inhibition" or "promotion" are inadequate and even misleading descriptors of the effect of external agents on fibrillogenesis. For example, conditions inhibiting nucleation could be interpreted both as "inhibiting" fibrillogenesis, since the total number of fibers will be small, and as "promoting" it, since longer fibrils will be formed. Similarly, conditions promoting nucleation could be interpreted as "promoting" fibrillogenesis because fibers will be more numerous and as "inhibiting" it because shorter fibers will be formed. It has been suggested that these considerations also apply to Aβ polymerization (29). Therefore, a complete characterization of Aβ fibrillogenesis must include quantitation of both fibril concentration and fibril dimensions throughout the polymerization process.

Previous efforts (12–14, 23) to investigate the kinetics of Aβ fibrillogenesis have had methodological limitations. CD and Fourier-transform IR spectroscopies, turbidity, or thioflavin T binding could not provide direct information on fibril size, while EM, which could elucidate fibril dimensions, was not appropriate for real-time kinetic studies. In contrast, quasi-elastic light-scattering spectroscopy (QLS) was long recognized as a powerful tool for the study of aggregation kinetics (30). However, since Aβ fibrillogenesis occurs very rapidly at neutral pH, previous applications of QLS to the Aβ problem

The publication costs of this article were defrayed in part by page charge payment. This article must therefore be hereby marked "*advertisement*" in accordance with 18 U.S.C. §1734 solely to indicate this fact.

Abbreviations: Aβ, amyloid β-protein-(1–40) fragment; $C_{12}E_6$, *n*-dodecylhexaoxyethylene glycol monoether; QLS, quasi-elastic light-scattering spectroscopy.

[¶]Present address: Seoul National University, Seoul, Republic of Korea.
[‖]To whom reprint requests should be addressed.
[‡‡]Present address: Department of Biological Sciences, University of Massachusetts, Lowell, MA 01854.

(19, 20, 31, 32) have provided data primarily on later stages of the process. We report here the use of QLS to study Aβ fibrillogenesis in aqueous 0.1 M HCl, a milieu in which fibril growth was reproducible and sufficiently slow to allow detailed monitoring of the entire process of fibril growth, including the initial nucleation step. Based on these data, we developed a detailed kinetic model of Aβ fibrillogenesis that accounts for both the concentration and the lengths of fibrils as a function of time. This quantitative model permits a determination of the two key kinetic parameters describing Aβ polymerization: nucleation rate and elongation rate. As a result, our paradigm may be used to fully characterize the effects of endogenous molecules or potential therapeutic agents on Aβ fibrillogenesis.

MATERIALS AND METHODS

Peptide Synthesis and Characterization. Aβ [Aβ-(1–40)] was synthesized on an automated peptide synthesizer (Applied Biosystems model 430A) by 9-fluorenylmethoxycarbonyl-based methods. The identity and purity of the final product was confirmed by quantitative amino acid analysis, matrix-assisted laser desorption/ionization time-of-flight mass spectrometry, and reverse-phase high performance liquid chromatography.

QLS. Measurements were performed at 25°C with a 144-channel Langley Ford model 1097 correlator and either a Spectra-Physics model 164 argon laser (488 nm) or a Spectra-Physics model 127 helium–neon laser (633 nm). The scattering angle was 90°. Lyophilized Aβ was solubilized in 0.1 M HCl, gently mixed, and centrifuged at 5000 × *g* for 30 min to sediment any dust particles. Immediately after centrifugation and continuing for 20–50 hr, the intensity and the autocorrelation function of the scattered light were automatically measured for periods of 5–30 min. By 50 hr, fibril growth was typically finished. Some samples were kept at room temperature and reexamined periodically during the next few months. Protein concentrations were determined a posteriori by amino acid analysis. Experiments with *n*-dodecylhexaoxyethylene glycol monoether ($C_{12}E_6$; M_r = 450.7; Nikko Chemicals, Tokyo) were done in a similar fashion, except that Aβ was dissolved in 0.1 M HCl already containing the appropriate $C_{12}E_6$ concentration.

The size distribution of fibrils in solution was determined by a constrained regularization method (33) adapted to the analysis of the homodyne correlation function. The observed distribution of diffusion coefficients was relatively narrow; therefore, we present here the average hydrodynamic radii (R_h) of scattering particles. We have used the following interpolation, appropriate for a cylinder of length L and diameter d (34), to relate the experimentally measured R_h values to the fibril length:

$$R_h = \frac{L}{2}\cdot\left(\sqrt{1-x^2}\Big/\ln\frac{1+\sqrt{1-x^2}}{x}\right),$$

where

$$x = \frac{d}{L}\left[1 + \frac{0.37(L-d)}{L}\right].$$

Static Light Scattering. Following cessation of fiber growth, the intensity of light (488 nm) scattered from Aβ samples of concentration 0.025 mM and 0.28 mM was measured at 12 angles between 11.5° and 162.6°, as described (35). The measurements were normalized with respect to optical grade toluene (Rayleigh ratio = $39.6\cdot10^{-6}$ cm^{-1}; Aldrich), thereby permitting determination of the absolute value of the scattered light intensity.

EM. After QLS experiments were completed, sample cuvettes were gently agitated in a Vortex mixer, and then 10 μl of sample was spotted onto a Formvar grid for 1 min. The grid was then treated with 0.5% glutaraldehyde for 1 min, rinsed with water, and negatively stained for 2 min with 2% uranyl acetate. After drying, the grids were examined in a JEOL 1200 EX electron microscope at 120 kV. Fibril dimensions were determined by using tropomyosin paracrystals (provided by C. Cohen, Brandeis University).

CD Spectroscopy. Measurements were made at room temperature on an Aviv model 62 DS spectrometer using a 0.1-cm cuvette and a spectral range of ≈190–250 nm. The program CDANAL v. 1.0 (36) was used to determine the relative amounts of individual secondary structure elements.

RESULTS

Structure of Fibers Formed at Low pH. In aqueous 0.1 M HCl, fibrillogenesis was highly reproducible and amenable to detailed temporal monitoring by QLS (see below). Importantly, the morphology of the fibers produced under these conditions was highly similar to that observed in Alzheimer plaque amyloid (Fig. 1). The fibers were unbranched, straight, or slightly curved and had a diameter of 8 nm. Analysis of protein secondary structure by CD (data not shown) showed that the Aβ fibrils were composed predominantly (>90%) of parallel and antiparallel β-strand elements, including β-turns. Static light-scattering data (not shown) could be fit accurately by using the structure factor for rigid rods. Fibril length, L, was found to agree within an error of 20% with L determined by QLS analysis (see below). Fibril linear density, λ, was found to be 6.8 kDa/nm (1.6 Aβ monomers per nm), assuming a specific refractivity of Aβ peptide of 0.19 ml/g.

QLS Spectroscopy. To examine the concentration dependence of Aβ fibrillogenesis by QLS, 10 different initial peptide concentrations, C_0, in the range of ≈0.02–2.0 mM (≈0.08–8.0 mg/ml) were studied. In each case, fibril formation manifested itself as a temporal increase in the observed hydrodynamic radius, R_h, and in the intensity of the scattered light. The intensity grew proportionately to R_h, consistent with a fibrillar structure for the aggregates.

The kinetic evolution of fibrils exhibited two distinct patterns, depending on the concentration of the peptide. For $C_0 > 0.1$ mM, which we have designated the critical concentration, c^*, this evolution was independent of concentration (Fig. 2). Immediately after peptide dissolution, a structure with $R_h \approx 7$ nm was observed (Fig. 2 *Inset*). This structure was most evident at higher peptide concentration. As time proceeded, the hydrodynamic radius began to increase. The elongation rate remained nearly constant for ≈10 hr and then gradually

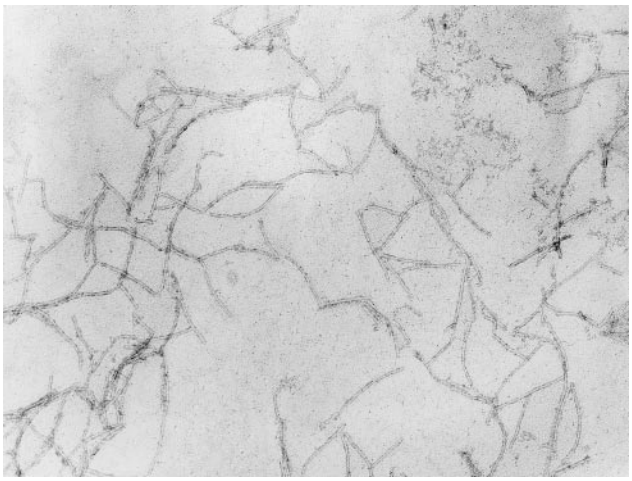

FIG. 1. Electron micrograph of Aβ fibrils formed at low pH. Synthetic Aβ-(1–40), 0.17 mM in 0.1 M HCl, was negatively stained and examined 76 days after dissolution. (×51,000.)

decreased. The final asymptotic size of 32 ± 2 nm (Fig. 2, dashed line) occurred after ≈4 days. This value of R_h corresponds to rigid rods of length ≈ 240 nm, assuming a diameter of 8 nm.

A different kinetic pattern was evident for $C_0 \leq 0.1$ mM (Fig. 3). Under these conditions, the rate of fibril growth increased with concentration. Extrapolation of the data from each of the four different Aβ concentrations back to $t = 0$ produced identical initial R_h values of ≈4 nm. Indeed, for fibers formed when $C_0 > 0.1$ mM, extrapolation of data from the time domain in which the fiber elongation rate was constant back to $t = 0$ also yielded the same value of 4 nm (Fig. 2).

Though the initial growth rate of the fibrils for $C_0 < c^*$ was smaller than that found for concentrations greater than c^*, the final asymptotic size was significantly larger than 32 nm. We converted values for the hydrodynamic radius, R_h, into fibril length, L_f, and calculated the initial growth rate, dL/dt (Fig. 4 *Upper*). This rate was independent of concentration for $C_0 > c^*$ but decreased linearly with concentration as C_0 fell below c^*.The final fibril length, when $C_0 > c^*$, was 240 ± 20 nm but was significantly greater when $C_0 < c^*$ (Fig. 4 *Lower*).

QLS-Based Fibrillogenesis Assay. To assess the usefulness of QLS in detecting and monitoring alterations of the kinetics produced by exogenous solutes, we examined the effect of the surfactant $C_{12}E_6$ on Aβ fibrillogenesis (Fig. 5). At a $C_{12}E_6$/Aβ ratio of 1:2.5, $C_{12}E_6$ had a negligible effect on the initial growth rate. However, the final R_h in this case was >50 nm, compared with 32 nm in the absence of $C_{12}E_6$. At a ratio of 1:1, we observed a nearly 50% reduction in the initial elongation rate. This reduction became even more prominent as the surfactant/Aβ ratio rose to 20:1. These data suggest that the QLS method could serve as an effective tool in the search for reagents that alter Aβ aggregation.

DISCUSSION

Our data indicate that the process of Aβ fibrillogenesis is different depending on whether the initial protein concentration, C_0, is less than or greater than a critical concentration, c^*. We propose that a different mechanism of fibril nucleation predominates in each concentration domain (Fig. 6). In our model, the key factor in fibrillogenesis for $C_0 > c^*$ is the spontaneous self-assembly of Aβ monomers into micelles. Micelle formation is typical of surfactant solutions (37); in fact, surfactant properties of Aβ have been demonstrated in surface tension studies (38). We propose that c^* is the critical micelle concentration (cmc) of Aβ. When $C_0 > c^*$ (Fig. 6*A*), a reversible equilibrium between monomers and micelles is rapidly established. Since micelles are regions of high peptide concentration, we assume they serve as sites for the nucleation of Aβ fibrils. We denote the rate at which one nucleus emerges from one micelle as K_n (sec^{-1}). Alternative pathways, including heterogeneous nucleation (seeding on impurities), may also exist for the formation of fibril nuclei. When $C_0 < c^*$, no micelles are formed, and these alternative nucleation pathways predominate (Fig. 6*B*). Regardless of the mechanism of nucleation, our model posits that the fiber elongation rate is proportional to the solution monomer concentration, C, and has a rate constant K_e. Thus, each fibril grows at a rate of K_eC

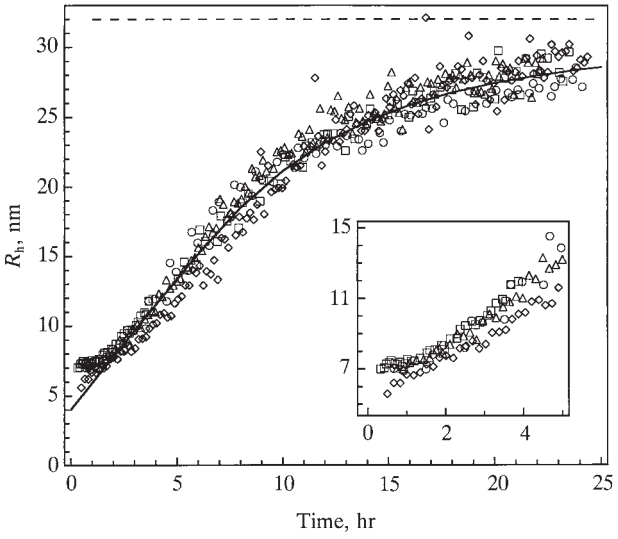

FIG. 2. Temporal evolution of the hydrodynamic radius (R_h) of Aβ fibrils in the concentration domain $C_0 > c^*$. ◇, C_0 = 0.17 mM; △, C_0 = 0.28 mM; ○, C_0 = 0.47 mM; □, C_0 = 1.7 mM. The dashed line indicates the universal asymptotic size of the fibrils. (*Inset*) The initial time domain is expanded to illustrate the 7-nm structures (micelles) observed upon dissolution of Aβ at high concentration.

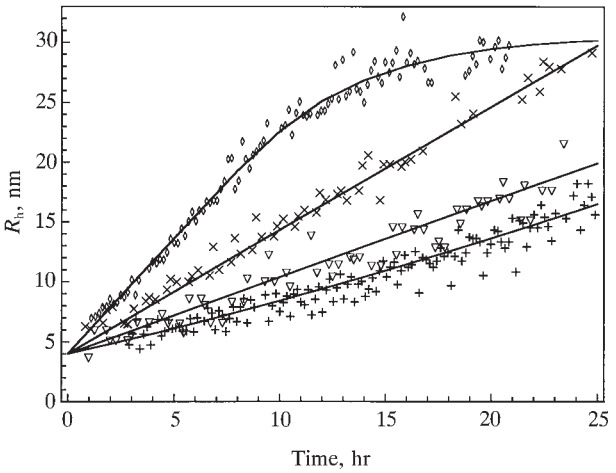

FIG. 3. Temporal evolution of the hydrodynamic radius (R_h) of Aβ fibrils in the concentration domain $C_0 \leq c^*$. ◇, C_0 = 0.11 mM; ×, C_0 = 0.058 mM; ▽, C_0 = 0.028 mM; +, C_0 = 0.025 mM.

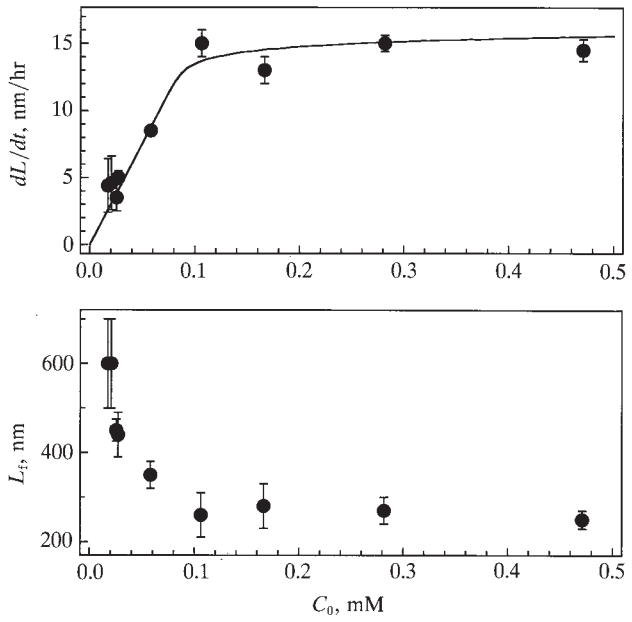

FIG. 4. Concentration dependence of fibril growth. (*Upper*) The initial rate of elongation of fibrils, dL/dt, determined in the time domain where growth was linear, as a function of C_0. The solid line represents the concentration dependence of the theoretical initial elongation rate K_eC/λ for $c^* = 0.1$ mM, $m = 25$, and $K_e = 65$ M^{-1}·sec^{-1}. (*Lower*) The final length of fibrils, L_f, as a function of C_0.

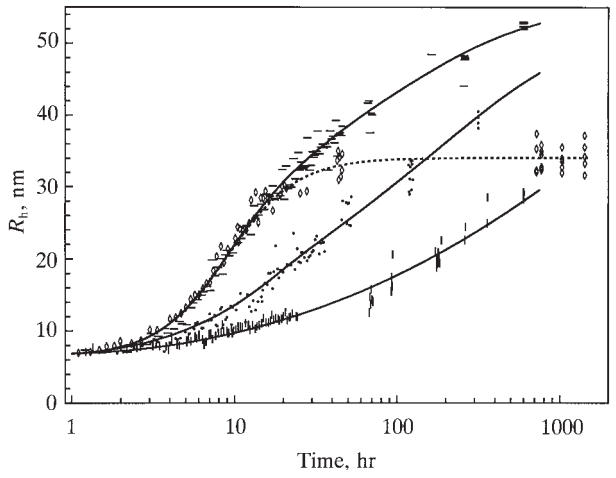

FIG. 5. Temporal evolution of the hydrodynamic radius (R_h) of Aβ fibrils in the presence of the surfactant $C_{12}E_6$. Aβ was dissolved at a concentration of ≈0.11 mM in 0.1 M HCl containing the following concentrations of $C_{12}E_6$: ◇, 0.00 mM; – (top curve), 0.044 mM; ●, 0.11 mM; and | (bottom curve), 2.2 mM. The dashed curve highlights the behavior of the sample without $C_{12}E_6$.

monomers per sec. Thus, it is important to understand the factors that control C during the process of fibril formation.

In the concentration domain $C_0 < c^*$, the initial concentration of Aβ monomers is essentially equal to the total concentration of dissolved peptide. The number of growing fibers remains equal to the number of heterogeneous nuclei initially present in the sample. Due to the binding of monomers to fibrils, C decreases exponentially with a time constant $(K_e N_f)^{-1}$, where N_f is the number of growing fibrils per unit volume, resulting in the gradual slowing of fibril growth.

In the concentration domain $C_0 > c^*$, micelles are formed. An important feature of the micelle–monomer equilibrium is that it maintains an almost constant monomer concentration slightly above the critical micelle concentration c^*. The initial rate of growth of fibrils is thus also constant, approximately equal to $K_e c^*$, and is independent of the initial concentration C_0. As free monomers are incorporated into fibrils, the pool of micelles is depleted until, at a time T, all micelles have been converted into monomers. After this time, the monomer concentration, and therefore the growth rate as well, decrease exponentially (Fig. 2).

The time T can be estimated as follows. The final length, L_f, of the fibril is related to T by the formula $\lambda L_f = K_e c^* T$, where λ is the number of monomers per unit length in a fibril. On the other hand, after fibrillogenesis is complete, $\lambda L_f = C_0/N_f$.

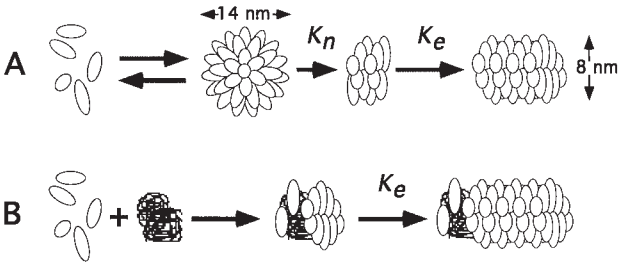

FIG. 6. Aβ fibrillogenesis at low pH. (*A*) Homogeneous nucleation and growth of Aβ fibrils for $C_0 > c^*$. Aβ monomers (ovoids) self-associate to form micelles (R_h = 7 nm, d = 14 nm), from which fibril nuclei (R_h = 4 nm, d = 8 nm) emerge at rate K_n. Aβ monomers add to the ends of these nuclei at rate K_e, producing fibrils of diameter 8 nm. (*B*) Heterogeneous nucleation and growth of Aβ fibrils for $C_0 < c^*$. In this concentration domain, nucleation occurs predominantly on non-Aβ seeds. The resulting fibrils are indistinguishable from those nucleated through micelles.

Thus, the micelle pool is exhausted at time $T = C_0/K_e c^* N_f$. N_f is determined by the number of nuclei formed from micelles during period T and is approximately equal to $K_n T C_0/m$, where m is the number of monomers per micelle and C_0/m, therefore, is the initial concentration of micelles. Substituting this expression for N_f into the equation for T, we find that $T = (K_e c^* K_n/m)^{-1/2}$, which is independent of the initial concentration C_0. Thus, the final length of fibrils is also independent of concentration and given by $\lambda L_f = (K_e c^*/K_n)^{1/2}$. The total number of fibrils is then given by $N_f = C_0(K_n/mK_e c^*)^{1/2}$. These results show that when nucleation is fast and elongation is slow, numerous short fibrils are formed. Conversely, when nucleation is slow and growth fast, the result is a small number of long fibrils.

We now can determine the numerical values of the parameters of our model. These parameters fall into two groups. The first group comprises the equilibrium and kinetic parameters c^*, K_n, and K_e. The second group describes geometrical features: the diameter, d, and the linear density, λ, of the fibril and the number of monomers per micelle, m. We have taken d = 8 nm and λ = 1.6 monomers per nm (see *Results*). This estimation of λ is consistent with the value 7.0 kDa/nm found previously for fibrils formed by Aβ-(1–39) at neutral pH (19). An accurate estimate of m is difficult to obtain; however, geometrical packing considerations and analysis of data in Fig. 4 *Upper* suggest that $15 < m < 70$.

To determine c^* and K_e, we need to examine the crossover between the domains where the initial growth rate is proportional to the initial concentration ($dL/dt = K_e C_0/\lambda$) and where it is independent of the initial concentration ($dL/dt = K_e c^*/\lambda$). From Fig. 4 *Upper*, we find that $K_e c^*/\lambda$ = 14.7 nm/hr, c^* = 0.1 mM, and consequently K_e = 65 $M^{-1}\cdot sec^{-1}$. The remaining parameter, K_n, can be determined from the concentration-independent final size observed in experiments with $C_0 > c^*$ (Fig. 4 *Lower*). For L_f = 240 nm, $\lambda K_n/m = 2.6\cdot10^{-4}$ $(nm\cdot hr)^{-1}$. By taking λ = 1.6 nm^{-1} and m = 25, $K_n = 1.1\cdot10^{-6}$ sec^{-1}, which corresponds to the emergence of one fiber nucleus per micelle in 9 days.

A central feature of our model is the formation of Aβ micelles that stabilize monomer concentration and provide sites for nucleation. We propose that these micelles correspond to the particles of R_h = 7 nm detected prior to significant fibril growth when $C_0 > c^*$ (Fig. 2). We also propose that the 4-nm hydrodynamic radius obtained by extrapolation to t = 0 corresponds to that of a fibril nucleus (Fig. 3). This would represent the first physical description of such a structure.

Micelles, in effect, control the conditions of fibril growth, permitting reproducible and precise QLS measurements that reveal the underlying features of Aβ fibrillogenesis. This suggested that our method could be used as an *in vitro* assay of the effects of solution additives or Aβ modifications on the parameters K_n, K_e, and c^*, which control Aβ fibrillogenesis. We demonstrated this assay potential in our study of the effect of $C_{12}E_6$ (Fig. 5). At the lowest $C_{12}E_6$ concentration, the final hydrodynamic radius was comparable to the value found in pure Aβ solutions when $C_0 < c^*$. In terms of our model, this behavior suggested that incorporation of $C_{12}E_6$ into Aβ micelles suppressed their ability to generate fibril nuclei to the point that heterogeneous nucleation dominated the nucleation process. Nevertheless, the initial growth rate was approximately equal to that found in the absence of $C_{12}E_6$, suggesting that c^* was, at least initially, unaffected by $C_{12}E_6$. On the other hand, as the $C_{12}E_6$:Aβ molar ratio approached unity, the initial growth rate decreased substantially. This was consistent with a mechanism in which $C_{12}E_6$ micelles sequestered Aβ and thereby reduced the monomer concentration.

Self-assembly of Aβ *in vivo* occurs in a biologic milieu characterized by dynamic equilibrium among processes of production, elimination, sequestration, and fibrillization of Aβ monomers. Regardless of this complexity of conditions, fibril-

logenesis must be controlled by the concentration of Aβ and by kinetic factors analogous to those described above. For example, homogeneous fibril nucleation is unlikely to occur in the plasma or cerebrospinal fluid because the concentration of Aβ in these compartments is very low. However, this may not be the case within lysosomes in which Aβ-(1–42) accumulates (39). Nucleation of Aβ fibrils might also be enhanced through association with apolipoprotein E4 (40) or with other molecules. Once nuclei are formed, fiber elongation proceeds at a rate proportional to the concentration of Aβ monomers. In Down syndrome patients with Alzheimer disease (40), for example, the relatively large senile plaques observed could result from increased production of Aβ. Other considerations relevant to Aβ fibrillogenesis include whether Aβ exists as a monomer or is complexed with other proteins and whether new fibril ends are created through enzymatic action within the plaque.

Clearly, the factors influencing the nucleation of fibrils and the rate of fibril growth *in vivo* are complex and numerous, yet the model we have presented provides a basis for examination of the precise roles of each of these factors in fibrillogenesis. We have shown here that the kinetic parameters describing Aβ fibrillogenesis can readily be deduced from data obtained by QLS. We thus now possess the theoretical and experimental tools with which to investigate systematically the underlying molecular mechanisms of Aβ fibrillogenesis.

We thank Ms. Margaret Condron and Ms. Karen Szumowski for expert technical assistance and Drs. Dominic Walsh and Eddie Koo for critical comment. This work was supported by an Alzheimer's Association Zenith Award (to D.A.K.) and by National Institutes of Health Grants NIH-NIAAG 08572 (to D.A.K.) and NIH-5-R37-EYO5127 (to G.B.B.).

1. Selkoe, D. J. (1994) *Annu. Rev. Cell Biol.* **10,** 373–403.
2. Selkoe, D. J. (1993) *Trends Neurosci.* **16,** 403–409.
3. Haass, C., Hung, A. Y., Citron, M., Teplow, D. B. & Selkoe, D. J. (1995) *Arzneim. Forsch.* **45,** 398–402.
4. Higaki, J., Quon, D., Zhong, Z. Y. & Cordell, B. (1995) *Neuron* **14,** 651–659.
5. Seubert, P., Vigo-Pelfrey, C., Esch, F., Lee, M., Dovey, H., Davis, D., Sinha, S., Schlossmacher, M. G., Whaley, J., Swindlehurst, C., McCormack, R., Wolfert, R., Selkoe, D. J., Lieberburg, I. & Schenk, D. (1992) *Nature (London)* **359,** 325–327.
6. Shoji, M., Golde, T. E., Ghiso, J., Cheung, T. T., Estus, S., Shaffer, L. M., Cai, X., McKay, D. M., Tintner, R., Frangione, B. & Younkin, S. G. (1992) *Science* **258,** 126–129.
7. Haass, C., Schlossmacher, M. G., Hung, A. Y., Vigo-Pelfrey, C., Mellon, A., Ostaszewski, B. L., Lieberburg, I., Koo, E. H., Schenk, D., Teplow, D. B. & Selkoe, D. J. (1992) *Nature (London)* **359,** 322–325.
8. Busciglio, J., Gabuzda, D. H., Matsudaira, P. & Yankner, B. A. (1993) *Proc. Natl. Acad. Sci. USA* **90,** 2092–2096.
9. Narang, H. K. (1980) *J. Neuropathol. Exp. Neurol.* **39,** 621–631.
10. Merz, P. A., Wisniewski, H. M., Somerville, R. A., Bobin, S. A., Masters, C. L. & Iqbal, K. (1983) *Acta Neuropathol.* **60,** 113–124.
11. Kirschner, D. A., Abraham, C. & Selkoe, D. J. (1986) *Proc. Natl. Acad. Sci. USA* **83,** 503–507.
12. Kirschner, D. A., Inouye, Y., Duffy, L. K., Sinclair, A., Lind, M. & Selkoe, D. J. (1987) *Proc. Natl. Acad. Sci. USA* **84,** 6953–6957.
13. Fraser, P. E., Nguyen, J. T., Surewicz, W. K. & Kirschner, D. A. (1991) *Biophys. J.* **60,** 1190–1201.
14. Hilbich, C., Kisters-Woike, B., Reed, J., Masters, C. & Beyreuther, K. (1991) *J. Mol. Biol.* **218,** 149–163.
15. Barrow, C. J., Yasuda, A., Kenny, P. T. M. & Zagorski, M. (1992) *J. Mol. Biol.* **225,** 1075–1093.
16. Fraser, P. E., Nguyen, J. T., Inouye, H., Surewicz, W. K., Selkoe, D. J., Podlisny, M. B. & Kirschner, D. A. (1992) *Biochemistry* **31,** 10716–10723.
17. Burdick, D., Soreghan, B., Kwon, M., Kosmoski, J., Knauer, M., Henschen, A., Yates, J., Cotman, C. & Glabe, C. (1992) *J. Biol. Chem.* **267,** 546–554.
18. Snyder, S. W., Ladror, U. S., Wade, W. S., Wang, G. T., Barrett, L. W., Matayoshi, E. D., Huffaker, H. J., Krafft, G. A. & Holzman, T. F. (1994) *Biophys. J.* **67,** 1216–1228.
19. Shen, C.-L., Fitzgerald, M. C. & Murphy, R. M. (1994) *Biophys. J.* **67,** 1238–1246.
20. Shen, C.-L. & Murphy, R. M. (1995) *Biophys. J.* **69,** 640–651.
21. Wisniewski, T., Castano, E. M., Golabek, A., Vogel, T. & Frangione, B. (1994) *Am. J. Pathol.* **145,** 1030–1035.
22. Ma, J. Y., Yee, A., Brewer, H. B., Das, S. & Potter, H. (1994) *Nature (London)* **372,** 92–94.
23. Evans, K. C., Berger, E. P., Cho, C. G., Weisgraber, K. H. & Lansbury, P. T. (1995) *Proc. Natl. Acad. Sci. USA* **92,** 763–767.
24. Fraser, P. E., Nguyen, J. T., McLachlan, D. R., Abraham, C. R. & Kirschner, D. A. (1993) *J. Neurochem.* **61,** 298–305.
25. Eriksson, S., Janciauskiene, S. & Lannfelt, L. (1995) *Proc. Natl. Acad. Sci. USA* **92,** 2313–2317.
26. Tobacman, L. S. & Korn, E. D. (1983) *J. Biol. Chem.* **258,** 3207–3214.
27. Pollard, T. D. & Cooper, J. A. (1986) *Annu. Rev. Biochem.* **55,** 987–1035.
28. Fesce, R., Benfenati, F., Greengard, P. & Valtorta, F. (1992) *J. Biol. Chem.* **267,** 11289–11299.
29. Jarrett, J. T. & Lansbury, P. T., Jr. (1993) *Cell* **73,** 1055–1058.
30. Cohen, R. J. & Benedek, G. B. (1975) *Immunochemistry* **12,** 349–351.
31. Tomski, S. J. & Murphy, R. M. (1992) *Arch. Biochem. Biophys.* **294,** 630–638.
32. Shen, C.-L., Scott, G. L., Merchant, F. & Murphy, R. M. (1993) *Biophys. J.* **65,** 2383–2395.
33. Braginskaya, T. G., Dobitchin, P. D., Ivanova, M. A., Klyubin, V. V., Lomakin, A. V., Noskin, V. A., Shmelev, G. E. & Tolpina, S. P. (1983) *Phys. Scripta* **28,** 73–79.
34. de la Torre, J. G. & Bloomfield, V. A. (1981) *Q. Rev. Biophys.* **14,** 81–139.
35. Schurtenberger, P., Chamberlin, R. A., Thurston, G. M., Thomson, J. A. & Benedek, G. B. (1989) *Phys. Rev. Lett.* **63,** 2064–2067.
36. Perczel, A., Park, K. & Fasman, G. D. (1992) *Anal. Biochem.* **203,** 83–93.
37. Tanford, C. (1973) *The Hydrophobic Effect: Formation of Micelles and Biological Membranes* (Wiley, New York).
38. Soreghan, B., Kosmoski, J. & Glabe, C. (1994) *J. Biol. Chem.* **269,** 28551–28554.
39. Yang, A. J., Knauer, M., Burdick, D. A. & Glabe, C. (1995) *J. Biol. Chem.* **270,** 14786–14792.
40. Hyman, B. T., West, H. L., Rebeck, G. W., Buldyrev, S. V., Mantegna, R. N., Ukleja, M., Havlin, S. & Stanley, H. E. (1995) *Proc. Natl. Acad. Sci. USA* **92,** 3586–3590.